HHS Public Access

Author manuscript

Cell Rep. Author manuscript; available in PMC 2017 December 29.

Published in final edited form as:

Cell Rep. 2017 December 26; 21(13): 3691–3699. doi:10.1016/j.celrep.2017.12.004.

Rlim-dependent and -independent pathways for X chromosome inactivation in female ESCs

Feng Wang[1], **Kurtis N. McCannell**[1], **Ana Bošković**[2], **Xiaochun Zhu**[1], **JongDae Shin**[1,†], **Jun Yu**[1], **Judith Gallant**[3], **Meg Byron**[3], **Jeanne B. Lawrence**[3], **Lihua J. Zhu**[1,4,5], **Stephen N. Jones**[3,#], **Oliver J. Rando**[2], **Thomas G. Fazzio**[1,4], and **Ingolf Bach**[1,4,*]

[1]Department of Molecular, Cell and Cancer Biology, University of Massachusetts Medical School, Worcester, MA 01605

[2]Department of Biochemistry and Molecular Pharmacology, University of Massachusetts Medical School, Worcester, MA 01605

[3]Department of Cell and Developmental Biology, University of Massachusetts Medical School, Worcester, MA 01605

[4]Program in Molecular Medicine, University of Massachusetts Medical School, Worcester, MA 01605

[5]Program in Bioinformatics and Integrative Biology, University of Massachusetts Medical School, Worcester, MA 01605

SUMMARY

During female mouse embryogenesis, two forms of X chromosome inactivation (XCI) ensure dosage compensation from sex chromosomes. Beginning at the four-cell stage, imprinted XCI (iXCI) exclusively silences the paternal X (Xp), and this pattern is maintained in extraembryonic cell types. Epiblast cells, which give rise to the embryo proper, reactivate the Xp (XCR) and undergo a random form of XCI (rXCI) around implantation. Both iXCI and rXCI is dependent on the long non-coding RNA *Xist*. The ubiquitin ligase RLIM is required for iXCI *in vivo* and occupies a central role in current models of rXCI. Here, we demonstrate the existence of *Rlim*-

[*]Corresponding author and Lead contact: Tel: 508 856 5627, Fax: 508 856 4650, ingolf.bach@umassmed.edu.
[†]Current address
Department of Cell Biology, College of Medicine, Konyang University, Daejeon, Korea
[#]Current address
Frederick National Laboratory for Cancer Research, Frederick, MD 21702

Author contributions

Conceptualization: I.B. and F.W.; Methodology: F.W., K.N.M., A.B., J.Y., J.S., J.G., M.B., and X.Z.; Investigation: F.W., K.N.M., A.B., J.Y., J.S., J.G., M.B., X.Z., and I.B.; Supervision: I.B., T.G.F., O.J.R., S.N.J., L.J.Z. and J.B.L.; Writing: I.B., F.W., K.M.N., and T.G.F.

Declaration of interests

The authors declare no competing interests.

Accession numbers

RNA-seq data have been deposited with the GEO repository (GSE101838).

dependent and -independent pathways for rXCI in differentiating female ESCs. Upon uncoupling these pathways we find more efficient *Rlim*-independent XCI in ESCs cultured under physiological oxygen conditions. Our results revise current models of rXCI and suggest that caution must be taken when comparing XCI studies in ESCs and mice.

Graphical Abstract

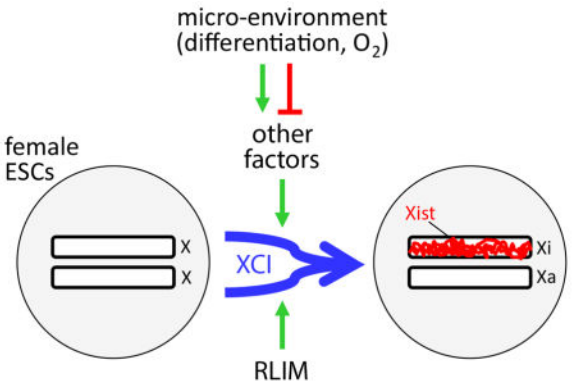

INTRODUCTION

Female mammalian embryogenesis and reproduction is critically dependent on a process called X chromosome inactivation (XCI), which silences one of the two sex chromosomes to achieve dosage compensation. XCI serves as a paradigm to study the epigenetic regulation, whereby gene expression states are maintained independent of DNA sequence. In mice, an imprinted form of XCI (iXCI) is initiated in embryos at the 4-cell stage silencing exclusively the paternal X (Xp), and this XCI pattern is maintained in extraembryonic tissues. However, epiblast cells, which give rise to the embryo proper, experience a major epigenetic switch around implantation: These cells reactivate the Xp and undergo a random form of XCI (rXCI), in which the Xp or the maternal X (Xm) is inactivated in each cell with equal probability. Both forms of XCI require the long non-coding *Xist* RNA which forms clouds on the inactive X chromosome (Xi) from which it is transcribed, leading to X-silencing. The X-linked gene *Rlim* (also known as *Rnf12*) has emerged as a critical mediator of *Xist* activity. *Rlim* encodes a ubiquitin ligase (E3) (Ostendorff et al., 2002) that is involved in transcriptional regulation (Bach et al., 1999; Gontan et al., 2012; Gungor et al., 2007) and shuttles between the nucleus and cytoplasm (Jiao et al., 2013). In mice, a maternally transmitted *Rlim*KO allele (m) results in early lethality of female embryos in a sex-specific parent-of-origin effect due to a failure to maintain iXCI and *Xist* clouds (Shin et al., 2010; Wang et al., 2016). In contrast, loss of *Rlim* in female epiblast cells has minimal effect on the rXCI process. Indeed, RLIM protein levels are downregulated specifically in epiblast cells of implanting embryos, consistent with the lack of rXCI phenotype in *Rlim* mutant females (Shin et al., 2014). These data identify *Rlim*-dependent and -independent mechanisms of XCI *in vivo* that separately act in pre-implantation embryos and epiblasts, respectively. However, *Rlim* is crucial for XCI in female ESCs differentiated in culture (Barakat et al., 2011; Barakat et al., 2014).

To further investigate mechanisms of rXCI we generated female ESCs with a homozygous *Rlim*KO. We found that these cells undergo XCI *in vivo*, but XCI *in vitro* is strongly influenced by culture conditions, including both the method of differentiation and O_2 levels. Our results demonstrate *Rlim*-dependent and -independent pathways for XCI exist in ESCs and, together with published data, profoundly change current models of X dosage compensation.

RESULTS

Female ESCs lacking RLIM undergo XCI *in vivo*

Genetic evidence indicates that iXCI in female pre-implantation embryos requires RLIM, but that activation of *Xist* during rXCI in the female epiblast is *Rlim*-independent (Shin et al., 2010; Shin et al., 2014). Indeed, *Xist* clouds form specifically in the ICM of female blastocyst outgrowths with a maternal *Rlim* deletion (Δm) (Shin et al., 2010), consistent with a critical role for RLIM in iXCI but not rXCI. To exclude any influence of RLIM on rXCI, we examined Δm/Δp female blastocysts generated by crossing Δ/Y males with Sox2-Cre (SC) - cKO_m/Δ_p dams, which lack RLIM both in somatic tissues and germline (Wang et al., 2016). E4 blastocysts generated by this cross were cultured for 3 days and analyzed by RNA FISH. Indeed, *Xist* clouds were readily detectable specifically in cells of the ICM in female Δ/Δ blastocyst outgrowths (Fig. 1A), consistent with *Rlim*-independent induction of rXCI *in vivo*.

Newly isolated primary female ESCs that lack RLIM activate *Xist* and form *Xist* clouds upon differentiation *in vitro* (Shin et al., 2010; Shin et al., 2014). However, in a female ESC line with a homozygous *Rlim* KO (Rnf12KO) XCI was blocked upon ESC differentiation (Barakat et al., 2011), suggesting that XCI is induced in a context-dependent manner. Because primary female *Rlim*KO ESCs proved unstable upon prolonged culture, to investigate mechanisms of XCI, we generated three independent ESC lines lacking RLIM via CRISPR/Cas9 technology (Fig. 1B) using the established mouse PGK12.1 female ESC model (Norris et al., 1994). Sequencing confirmed homozygous frameshift mutations in exon 3, the first coding exon in *Rlim* (Fig. S1A). We named these lines *Rlim*16p, *Rlim*23p and *Rlim*27p, reflecting the amino acid position where each frame shift occurred as well as the ESC origin (p, PGK12.1). Consistent with published results (Barakat et al., 2011), differentiation upon treatment with retinoic acid (RA) showed that XCI was *Rlim*-dependent, as development of *Xist* clouds and H3K27me3 foci was inhibited in *Rlim*KO ESCs, even after differentiating cells for 12d (Figs 1C, D; S1B, C). As previously reported (Barakat et al., 2011), we observed sporadic clusters of a few cells that displayed H3K27me3 foci in all KO lines (not shown), indicating that *Rlim*KO ESCs have the ability to undergo XCI, but do so at a very low rate. To further investigate the potential of *Rlim*KO ESCs for XCI, we examined their XCI capability *in vivo.* To allow lineage tracing, we used lentiviral infections to generate WT and *Rlim*KO ESC lines stably expressing GFP (lentivirus pWPT-GFP, Addgene) (Fig. S1D; not shown). Approximately 10–12 GFP-ESCs were microinjected in mouse pre-implantation embryos at E3.5. Injected embryos were surgically placed into the oviducts of pseudo-pregnant females and allowed to develop, and MEFs of E12.5 embryos were prepared and tested for GFP expression in ICC (Fig. 1E).

GFP-positive MEFs of independent embryos were isolated via FACS (6 each for WTp and *Rlim*16p, 3 for *Rlim*23p, and 1 for *Rlim*27p) and similar fractions of GFP-positive vs -negative MEFs obtained from individual embryos injected with *Rlim*16p or WTp ESCs were obtained (Fig. S1E). Testing for signs of XCI, around 40–50% of WT and KO GFP-MEFs developed H3K27me3 foci (Figs. 1F, G) and co-staining revealed more than 90% of MEFs with H3K27me3 foci displayed overlapping *Xist* clouds (Fig. S1F). In strand-specific RT-qPCR (ssRT-qPCR), we detected neither significant differences in *Xist* levels between *Rlim*KO and WT MEFs (Fig. S1G), nor in E10.5 female embryos with or without RLIM (fl_m/Δ_p and SC-cKO_m/Δ_p, respectively; Fig. S1H). Combined, these data show that female ESCs lacking RLIM cannot undergo XCI upon RA-differentiation, but can do so in the embryo, suggesting that environmental conditions influence XCI.

Rlim-dependent and -independent XCI in ESCs *in vitro*

Next, we compared XCI induced by RA-differentiation with embryoid body (EB) -differentiation in ESCs. Profiling protein expression in WT ESCs via Western blotting showed low levels of OCT4 by day 3 (d3) of differentiation, confirming ESC differentiation, whereas levels of RLIM by 6d were similar to those in undifferentiated ESCs (Fig. 2A). ssRT-qPCR analyses revealed that 6d EB-differentiated WT ESCs displayed less than 3-fold increased *Xist* levels when compared to RA-differentiated WT cells (Fig 2B). However, *Xist* levels in EB-differentiated *Rlim*KO ESCs were >50 fold higher under EB-differentiation relative to RA, with *Xist* clouds developing in a significant number of cells (Fig. 2C, D). Combined, these results provide the first evidence of *Rlim*-independent XCI in an established female ESC line, and show that differentiation conditions play a major role in *Rlim*-independent induction of *Xist*. Moreover, unlike in differentiating epiblast cells *in vivo* (Shin et al., 2014), differentiation of ESCs *in vitro* does not induce significant RLIM downregulation.

In another female ESC model, the KO of RLIM (*Rnf12*KO) resulted in complete inhibition of XCI, leading to far-reaching conclusions regarding *Rlim* function in rXCI (Barakat et al., 2011; Barakat et al., 2014). Because these results did not match our results (Fig. 2), we directly compared our *Rlim*KO ESC lines with the *Rnf12*KO cell line (Barakat et al., 2011). The *Rnf12*KO was achieved via insertion of foreign DNA into the *Rlim* gene at a position that might allow expression of a truncated RLIM protein consisting of the N-terminal 340 amino acids (Fig. S2A) (Jonkers et al., 2009). Indeed, Western blots using two independent RLIM antibodies detected a prominent band migrating at around 45kD (RLIM340) in these ESCs (Fig. 3A; S2B). Because of their F121 ESC background, we refer to this ESC line as *Rlim*340f. In agreement with published results (Gontan et al., 2012), REX1 levels in *Rlim*340f ESCs were increased (Fig. 3A). Interestingly, *Rlim*KOp ESCs displayed similar REX1 levels to WTp ESCs (Fig. 3A), indicating that in PGK12.1 ESCs RLIM is not solely responsible for regulating cellular REX1 levels. The predicted RLIM340 protein lacks the RING finger and nuclear export signal (NES) but retains part of the basic domain that mediates interactions with many substrate proteins, including REX1 (Fig. S2A) (Gontan et al., 2012; Ostendorff et al., 2002). ICC on undifferentiated *Rlim*340f ESCs revealed predominantly nuclear localization of the truncated RLIM protein (Fig. S2C), consistent with findings that RLIM lacking the NES is trapped in the nucleus (Jiao et al., 2013).

Moreover, forced expression of Myc-tagged RLIM340 in *Rlim*KOp ESCs via transient transfections revealed accumulation of endogenous REX1 protein in nuclei of transfected cells (Fig. 3B). However, in WT PGK12.1 cells expression of Myc-RLIM340 did not lead to REX1 accumulation, suggesting that the presence of the partial basic domain is not able to block interactions between full length RLIM and REX1.

To investigate the effects of RLIM340 expression on XCI, we induced frameshift mutations in *Rlim*340f ESCs via CRISPR/Cas9, using the same guide RNAs as for the *Rlim*KOp ESCs, yielding in independent ESCs carrying a homozygous KO of RLIM340, lines *Rlim*53f and *Rlim*0f (Figs. S2A; data not shown). Analysis of these lines via Western blot corroborated the KO and showed that the presence of RLIM340 did not significantly affect overall REX1 levels in undifferentiated ESCs (Fig. S2D). However, ICC staining confirmed that RLIM340 was critical to trap REX1 in the nucleus, as nuclear REX1 was significantly reduced in both KO lines relative to the *Rlim*340f line (Fig. 3C). Moreover, these KO ESCs performed XCI upon EB differentiation at a higher rate than *Rlim*340f cells, as measured by formation of *Xist* clouds (Fig. 3D). Combined, these results indicate gain-of-function activity of the truncated RLIM340, as opposed to dominant-negative functions. Consistent with findings that substrate proteins are often targeted by multiple E3 ligases mediated by interactions via the same/similar binding site (Bach and Ostendorff, 2003; Gungor et al., 2007), these results provide additional evidence that varying levels/repertoire of cellular competence factors in different ESC systems influences cellular REX1 levels and XCI.

Efficiency of *Rlim*-independent XCI *in vitro* is influenced by culture conditions

While the lack of RLIM does not affect overall rXCI efficiency *in vivo* (Figs. 1, S1), when compared to WT, *Rlim*KO ESCs undergo XCI with reduced efficiency upon EB-differentiation *in vitro* (Fig. 2) suggesting suboptimal culture conditions. *In utero,* ESCs differentiate in the context of extraembryonic cells and mammalian embryos are exposed to low O_2 levels (2–8%) (Fischer and Bavister, 1993). We therefore tested whether XCI efficiency of *Rlim*KO ESCs could be improved by mimicking these natural conditions. To test possible influences of extraembryonic cell types on XCI, we co-cultured EB-differentiating female GFP-*Rlim*KOp ESCs in the presence of a trophoblast stem cell line (TS) and/or a primitive endoderm (XEN) cell line (Niakan et al., 2013). However, this approach yielded no signs of improved XCI (not shown). To examine influences of O_2 levels on XCI, we compared *Xist* RNA levels and formation of clouds in *Rlim*KO ESCs with WTp ESCs, EB-differentiated and cultured in 7.5% O_2. Indeed, EB-differentiation in 7.5% O_2 resulted in a general increase of around two-fold in *Xist* levels and *Xist* cloud development in all *Rlim*KO ESC lines (Figs. 4A–D; not shown). While at 6d of differentiation *Rlim*16p ESCs appeared to develop similar XCI efficiencies when compared to WT, it was lower at 3d of EB-differentiation (Fig. S3A). No effects of 7.5% O_2 on XCI efficiency were observed on 6d RA-differentiated *Rlim*KO ESCs (not shown). Transcriptome analyses of undifferentiated and 6d EB-differentiated WTp, *Rlim*16p and E14 male ESCs via RNA-seq confirmed similar *Xist* levels in female ESCs (Fig. S3B), and comparisons of total X-linked transcripts versus total autosomal transcripts in differentiating WTp and mutant female ESC lines (relative to male E14) revealed similar global X-silencing in *Rlim*KOp and WTp ESCs (Figs. 4E, S3C). Because iXCI in female mice is *Rlim*-dependent, whereas rXCI occurs in

an *Rlim*-independent fashion, the identification of *Rlim*-dependent and –independent pathways for XCI in female ESCs illuminates mechanisms underlying X dosage compensation in female mice, including the epigenetic switch from iXCI to rXCI in epiblast cells (Fig. 4F).

DISCUSSION

Investigating XCI in female ESCs, we found that in an *in vivo* context, XCI in ESCs lacking *Rlim* occurs with similar efficiencies as in WT ESCs (Fig. 1), but *in vitro Rlim*-independent XCI is highly sensitive to the differentiation protocol as well as cell culture conditions (Figs. 2, 4). In particular, XCI in RA-differentiated ESCs is strictly *Rlim*-dependent (Fig. 2), indicating that this type of differentiation is not compatible with *Rlim*-independent XCI. Indeed, the formation of embryoid bodies more closely mimics the situation in blastocysts, and the finding that RLIM levels slightly increase during EB-differentiation (Fig. 2A) (Marks et al., 2015) is reminiscent of the increase in *Rlim* mRNA levels observed in early blastocysts, when the ICM forms (Wang et al., 2016). Moreover, we found that culturing differentiating ESCs in 7.5% O_2 levels had a general positive effect on *Rlim*-independent XCI efficiency (Fig. 4). Indeed, *in utero,* mammalian embryos are naturally exposed to low 2–8% O_2 levels (Fischer and Bavister, 1993), and atmospheric O_2 levels negatively influence development, global gene expression and XCI in cultured embryos/ESCs (Harvey et al., 2004; Lengner et al., 2010; Orsi and Leese, 2001). However, even in 7.5% O_2, the kinetics of XCI in *Rlim*KO cells is still slower than in WT ESCs (Fig. S3A), suggesting that these remain suboptimal XCI conditions. An alternative possibility is that the *Rlim*-independent XCI occurs more slowly upon induction of ESC differentiation. In this scenario, the presence of RLIM facilitates the more rapid XCI kinetics in WT ESCs. Combined, our results indicate elevated XCI efficiencies by the *Rlim*-independent pathway under conditions that more closely parallel conditions found *in vivo*. Thus, it will be interesting to identify the factor(s) and conditions that orchestrate rXCI in epiblasts in the future.

In contrast to epiblast cells of embryos undergoing rXCI, RLIM expression is maintained in differentiating ESCs (Fig. 2A). Thus, the *Rlim*-dependent pathway likely contributes towards XCI to varying degrees *in vitro*, depending on differentiation, culture conditions and likely also the specific ESC model used. The findings that 1) REX1 levels are not significantly affected by the *Rlim* deletion in PGK12.1 ESCs (Fig. 3A), 2) REX1 levels rapidly drop to undetectable levels within 24h of RA-differentiation in ESCs (Gontan et al., 2012; data not shown), and 3) the development of *Xist* clouds and H3K27me3 foci upon RA-differentiation is strictly *Rlim*-dependent (Fig. 1B, C), indicate that at least some functions of *Rlim* for XCI occur independent of REX1. However, the findings that in F121 ESCs, REX1 levels are affected by the presence/absence of RLIM (Gontan et al., 2012) and that *Rlim*-independent XCI in these ESCs is generally less efficient when compared to PGK12.1 ESCs (Fig. 4D), indicates that the cellular repertoire of expressed competency factors (e.g. E3 ligases) in different female ESC models has an important impact on XCI *in vitro*.

*Rlim*340f ESCs exhibit very low XCI activity and our results suggest that expression of the truncated RLIM340 might be a contributing factor, as it traps REX1 in the nucleus (Fig. 3),

and REX1 overall levels are strongly affected by RLIM in F121 ESCs (Gontan et al., 2012) but not in PGK12.1 ESCs (Fig. 3). Because RLIM regulates a variety of different factors by both RING-finger-dependent and -independent mechanisms (Her and Chung, 2009; Kramer et al., 2003; Ostendorff et al., 2002), it is likely that the activities of other nuclear proteins are altered in *Rlim*340f ESCs, with potential effect on XCI. Moreover, the specific epigenetic background in individual ESC lines may also contribute to XCI activity, as *Rlim*KO ESC lines undergo XCI with variable efficiencies. While it is clear that RLIM promotes XCI, our results indicate that *in vivo*, additional factors must be involved in proper counting of inactive X's, as previously proposed (Barakat et al., 2011; Jonkers et al., 2009). However, secondary roles for *Rlim* in rXCI in counting X's in mice with X chromosome abnormalities cannot be ruled out. In this context, it is important to point out the possibility that the gain-of-function activity of RLIM340 might contribute towards the skewed inactivation of the X harboring the mutated *Rlim* allele in *Rlim*340f heterozygous ESCs (Jonkers et al., 2009).

During mouse embryogenesis RLIM protein is detectable throughout preimplantation development, consistent with its functions in iXCI maintenance. However, in contrast to differentiating ESCs in culture (Fig. 2A), RLIM protein levels are downregulated in nuclei of epiblast cells of implanting embryos to levels that are undetectable by immunofluorescence (Shin et al., 2014). RLIM levels continue to remain low at early post-implantation stages through E7.5. At stage E8.5 RLIM protein levels are slowly upregulated in specific embryonic cell types, and by E11.5 RLIM protein is widely detectable in many tissues (Ostendorff et al., 2006)(data not shown). Thus, functions of *Rlim* in Xi maintenance at later embryonic stages and/or in mature tissue types are likely. The developmental expression pattern combined with the finding of *Rlim*-dependent and -independent XCI pathways in ESCs *in vitro* suggests a model for X dosage compensation in which *Rlim* occupies a major role to maintain *Xist* clouds and iXCI in cells of female embryos prior to XCR (Fig. 4G). While this role continues in extraembryonic tissues, RLIM is specifically downregulated in the epiblast lineage shortly before implantation thereby likely contributing to XCR, followed by induction of rXCI by an *Rlim*-independent pathway (Fig. 4G). This scenario is consistent with findings that *Rlim* is essential for the maintenance of iXCI, but dispensable for rXCI in epiblast cells. Moreover, it explains the precocious rXCI in epiblast cells of Δ/Δ blastocyst outgrowths (Fig. 1A), as, due to lack of iXCI, XCR is not required before induction of rXCI. Thus, iXCI in early female embryos and rXCI in epiblast cells are regulated by distinct pathways and the existence of *Rlim*-dependent and –independent pathways for XCI in female ESCs is likely the consequence of persistent RLIM expression upon differentiation *in vitro*.

Material and Methods

Cell culture and generation of PGK12.1 cell lines lacking RLIM

Female PGK12.1 and male E14 ESCs were cultured as described (Hooper et al., 1987; Norris et al., 1994). For RA differentiation, cells were plated at $2.5\times10^4/cm^2$ and cultured minus LIF with 100 nM retinoic acid (Sigma R2625) for 6 days. Embryoid bodies were formed in suspension by incubating cells in medium lacking LIF for 3 days on

bacteriological petri dishes, and after selection of smooth, spherical EBs, cells were differentiated attached to tissue culture dishes for the specified times. *Rlim* −/− PGK12.1 cell lines were generated by CRISPR/Cas9 cleavage (Cong et al., 2013; Mali et al., 2013) in exon 3. PGK12.1 cells were electroporated with pX330 (Cong et al., 2013) containing a puromycin resistance cassette for clonal selection, into which guideRNA oligonucleotides were cloned. Homozygous null mutations were confirmed by sequencing. GFP lines were generated by infection with pWPT-GFP lentivirus (Addgene). ESCs with a KO of RLIM340 (*Rlim*53f and *Rlim*0f) were generated based on Rnf12KO ESCs (Barakat et al., 2011) as described above except that pX330 with a hygromycin resistance cassette was used. Cells were cultured in 7.5% O_2 in a hypoxic chamber.

Oligonucleotides and RT-qPCR

Oligonucleotide	Sequence (5′ to 3′)
pX330-Rlim-1+	CACCAACAATTTGCTGGGCACCCC
pX330-Rlim-1−	AAACGGGGTGCCCAGCAAATTGTTC
Rlim-seq-f3:	AAGGCCCTAGGTTCACTTCC
Rlim-seq-r4	TATCCTCGACACCAAAGGCC
Rlim-seq-r2	AAGTGAGTTCCAGGACAGCT
Xist-ex6-ssRT	TGATCACGCTGAAGACCCAG
Xist-ex4/5-f	ACCCTACATCAAAGTAGGAGAAAAGC
Xist-ex6-r	TGTGCTGCTTTGGGGAAGG
Xist-ex4-ssRT	ACCTAGGGATCGTCAAGGG
Xist-ex2/3-f	TGGAGAGAGCCCAAAGGGAC
Xist-ex4-r	GCAGCAAGCCCACAATTCTG
Gapdh-ssRT	GGAAGCTTGTCATCAACGGG
Gapdh_q_f	CCAGCCTCGTCCCGTAGAC
Gapdh_q_r	GCCTTGACTGTGCCGTTGA

For ssRT-qPCR, RNA was isolated using TRIzol (Ambion) and treated with DNase1 (New England Biolabs). cDNA was synthesized with reverse transcriptase and primers specific for *Xist* and *Gapdh*. qPCR was performed with KAPA SYBR FAST Universal qPCR Master Mix on a Eppendorf realplex^2. The absence of genomic DNA was verified in RT-minus reactions.

Generation of chimeric mouse embryos and preparation of MEFs

E3.5 stage blastocysts (C57BL/6J-Tyrc-2J/J strain) were microinjected with 12–15 individual ESCs. Injected blastocysts were surgically transferred into the uteri of pseudo pregnant recipient SW strain female mice. After recovery, the females were housed under standard vivarium conditions. Pregnant dams were sacrificed 10 days post-surgery and chimeric E12.5 embryos were recovered for preparation of MEFs (Shin et al., 2010). All mice were housed in the animal facility of UMMS, and utilized according to NIH guidelines and those established by the UMMS Institute of Animal Care and Usage Committee.

Blastocyst outgrowths and RNA fluorescence in situ hybridization (RNA FISH)

Mice were maintained on a C57BL/6 background and parental genotypes to generate embryos for blastocyst outgrowths were based on described mouse models (Shin et al., 2010; Shin et al., 2014). E4 blastocysts were generated by natural mating, cultured for 48–96h prior to RNA FISH and genotyped after image recording. All mice were housed in the animal facility of UMMS and utilized according to NIH guidelines and those established by the UMMS Institute of Animal Care and Usage Committee. RNA FISH experiments including probes have been described (Shin et al., 2010; Shin et al., 2014). The *Rlim* probe detects mRNAs transcribed from both wild type and KO alleles (Shin et al., 2010).

Antibodies, Western blots, Immunostaining and Transient Transfections

Primary antibodies were rabbit and guinea pig RLIM (Ostendorff et al., 2002; Ostendorff et al., 2006), H3K27me3 (Abcam ab6002, Millipore 07-447), GFP (Rockland 600-101-215), REX1 (Abcam ab28141), Myc (Sigma 9E10), OCT4 (Santa Cruz sc-8628) and β-actin (Sigma A1978 and A5316). Secondary antibodies were Alexa Fluor® 488 Donkey Anti-Rabbit IgG (Invitrogen, A21206), Alexa Fluor® 488 Goat Anti-mouse IgG (Invitrogen, A11029), Alexa Fluor® 546 Goat Anti-Guinea Pig IgG (Invitrogen A11074), Alexa Fluor® 568 Goat Anti-Rabbit IgG (Invitrogen, A11011), Goat Anti-Rabbit IgG-HRP (Bio-Rad 170-6515), Goat Anti-Mouse IgG-HRP (Bio-Rad 170-6516), and Donkey Anti-Goat IgG-HRP (Santa Cruz Biotechnology sc-2020). Whole cell lysates for Western blots were prepared by lysing cells in WE16th lysis buffer (25 mM Tris, pH 7.5, 125 mM NaCl, 2.5 mM EDTA, 0.05% SDS, 0.5% NP-40, 10% glycerol). Transient transfections of RLIM340 (in pCS2MT) were carried out using FuGENE HD Transfection Reagent (Promega).

RNA-seq and data analyses

RNA-seq on ESC lines was essentially performed as described (Vallaster et al., 2017), and libraries were sequenced on a NextSeq 500 platform from Illumina, Inc. Quality-controlled reads were aligned to the mouse genome (Mus musculus/mm10) using TopHat (version 2.0.12) (Trapnell et al., 2009), with default setting except set parameter read-mismatches to 2, followed by running HTSeq (version 0.6.1p1) (Anders et al., 2015), Bioconductor packages edgeR (version 3.10.0) (Robinson et al., 2010; Robinson and Smyth, 2007) for differential gene expression analysis, and ChIPpeakAnno (version 3.2.0) (Zhu, 2013) for annotation. edgeR and Trimmed Mean of M-value (TMM) was used as described (Wang et al., 2016).

Statistical analyses

Student’s t tests were used to calculate statistical differences between individual groups via Microsoft Excel. p values < 0.05 were considered statistically significant.

Supplementary Material

Refer to Web version on PubMed Central for supplementary material.

Acknowledgments

We are grateful to M. Green, S. Bhatnagar and J. Gribnau, C. Gontan for providing PGK12.1 and Rnf12KO (*Rlim*340f) ESCs, respectively, and K. Hadjantonakis for TS and XEN cells. We thank M. Keeler for assistance in the UMMS Transgenic Animal Modeling Core, and S. Sissaoui and N. Lawson for the pWPT-GFP vector. I.B. is a member of the University of Massachusetts DERC (DK32520). This work was supported from NIH grants R01CA131158 to I.B., R01HD072122 to T. Fazzio, R01HD080224 and DP1ES025458 to O. Rando, R01CA077735 to S.N.J. and R01GM053234 to J.B.L.

References

Anders S, Pyl PT, Huber W. HTSeq--a Python framework to work with high-throughput sequencing data. Bioinformatics. 2015; 31:166–169. [PubMed: 25260700]

Bach I, Ostendorff HP. Orchestrating nuclear functions: ubiquitin sets the rhythm. Trends in biochemical sciences. 2003; 28:189–195. [PubMed: 12713902]

Bach I, Rodriguez-Esteban C, Carriere C, Bhushan A, Krones A, Rose DW, Glass CK, Andersen B, Izpisua Belmonte JC, Rosenfeld MG. RLIM inhibits functional activity of LIM homeodomain transcription factors via recruitment of the histone deacetylase complex. Nature genetics. 1999; 22:394–399. [PubMed: 10431247]

Barakat TS, Gunhanlar N, Pardo CG, Achame EM, Ghazvini M, Boers R, Kenter A, Rentmeester E, Grootegoed JA, Gribnau J. RNF12 activates Xist and is essential for X chromosome inactivation. PLoS genetics. 2011; 7:e1002001. [PubMed: 21298085]

Barakat TS, Loos F, van Staveren S, Myronova E, Ghazvini M, Grootegoed JA, Gribnau J. The Trans-Activator RNF12 and Cis-Acting Elements Effectuate X Chromosome Inactivation Independent of X-Pairing. Molecular cell. 2014; 53:965–978. [PubMed: 24613346]

Cong L, Ran FA, Cox D, Lin S, Barretto R, Habib N, Hsu PD, Wu X, Jiang W, Marraffini LA, et al. Multiplex genome engineering using CRISPR/Cas systems. Science. 2013; 339:819–823. [PubMed: 23287718]

Fischer B, Bavister BD. Oxygen tension in the oviduct and uterus of rhesus monkeys, hamsters and rabbits. J Reprod Fertil. 1993; 99:673–679. [PubMed: 8107053]

Gontan C, Achame EM, Demmers J, Barakat TS, Rentmeester E, van IW, Grootegoed JA, Gribnau J. RNF12 initiates X-chromosome inactivation by targeting REX1 for degradation. Nature. 2012; 485:386–390. [PubMed: 22596162]

Gungor C, Taniguchi-Ishigaki N, Ma H, Drung A, Tursun B, Ostendorff HP, Bossenz M, Becker CG, Becker T, Bach I. Proteasomal selection of multiprotein complexes recruited by LIM homeodomain transcription factors. Proceedings of the National Academy of Sciences of the United States of America. 2007; 104:15000–15005. [PubMed: 17848518]

Harvey AJ, Kind KL, Pantaleon M, Armstrong DT, Thompson JG. Oxygen-regulated gene expression in bovine blastocysts. Biology of reproduction. 2004; 71:1108–1119. [PubMed: 15163614]

Her YR, Chung IK. Ubiquitin Ligase RLIM Modulates Telomere Length Homeostasis through a Proteolysis of TRF1. The Journal of biological chemistry. 2009; 284:8557–8566. [PubMed: 19164295]

Hooper M, Hardy K, Handyside A, Hunter S, Monk M. HPRT-deficient (Lesch-Nyhan) mouse embryos derived from germline colonization by cultured cells. Nature. 1987; 326:292–295. [PubMed: 3821905]

Jiao B, Taniguchi-Ishigaki N, Gungor C, Peters MA, Chen YW, Riethdorf S, Drung A, Ahronian LG, Shin J, Pagnis R, et al. Functional activity of RLIM/Rnf12 is regulated by phosphorylation-dependent nucleocytoplasmic shuttling. Molecular biology of the cell. 2013; 24:3085–3096. [PubMed: 23904271]

Jonkers I, Barakat TS, Achame EM, Monkhorst K, Kenter A, Rentmeester E, Grosveld F, Grootegoed JA, Gribnau J. RNF12 is an X-Encoded dose-dependent activator of X chromosome inactivation. Cell. 2009; 139:999–1011. [PubMed: 19945382]

Kramer OH, Zhu P, Ostendorff HP, Golebiewski M, Tiefenbach J, Peters MA, Brill B, Groner B, Bach I, Heinzel T, et al. The histone deacetylase inhibitor valproic acid selectively induces proteasomal degradation of HDAC2. The EMBO journal. 2003; 22:3411–3420. [PubMed: 12840003]

Lengner CJ, Gimelbrant AA, Erwin JA, Cheng AW, Guenther MG, Welstead GG, Alagappan R, Frampton GM, Xu P, Muffat J, et al. Derivation of pre-X inactivation human embryonic stem cells under physiological oxygen concentrations. Cell. 2010; 141:872–883. [PubMed: 20471072]

Mali P, Yang L, Esvelt KM, Aach J, Guell M, DiCarlo JE, Norville JE, Church GM. RNA-guided human genome engineering via Cas9. Science. 2013; 339:823–826. [PubMed: 23287722]

Marks H, Kerstens HH, Barakat TS, Splinter E, Dirks RA, van Mierlo G, Joshi O, Wang SY, Babak T, Albers CA, et al. Dynamics of gene silencing during X inactivation using allele-specific RNA-seq. Genome biology. 2015; 16:149. [PubMed: 26235224]

Niakan KK, Schrode N, Cho LT, Hadjantonakis AK. Derivation of extraembryonic endoderm stem (XEN) cells from mouse embryos and embryonic stem cells. Nature protocols. 2013; 8:1028–1041. [PubMed: 23640167]

Norris DP, Patel D, Kay GF, Penny GD, Brockdorff N, Sheardown SA, Rastan S. Evidence that random and imprinted Xist expression is controlled by preemptive methylation. Cell. 1994; 77:41–51. [PubMed: 8156596]

Orsi NM, Leese HJ. Protection against reactive oxygen species during mouse preimplantation embryo development: role of EDTA, oxygen tension, catalase, superoxide dismutase and pyruvate. Molecular reproduction and development. 2001; 59:44–53. [PubMed: 11335946]

Ostendorff HP, Peirano RI, Peters MA, Schluter A, Bossenz M, Scheffner M, Bach I. Ubiquitination-dependent cofactor exchange on LIM homeodomain transcription factors. Nature. 2002; 416:99–103. [PubMed: 11882901]

Ostendorff HP, Tursun B, Cornils K, Schluter A, Drung A, Gungor C, Bach I. Dynamic expression of LIM cofactors in the developing mouse neural tube. Developmental dynamics: an official publication of the American Association of Anatomists. 2006; 235:786–791. [PubMed: 16395690]

Robinson MD, McCarthy DJ, Smyth GK. edgeR: a Bioconductor package for differential expression analysis of digital gene expression data. Bioinformatics. 2010; 26:139–140. [PubMed: 19910308]

Robinson MD, Smyth GK. Moderated statistical tests for assessing differences in tag abundance. Bioinformatics. 2007; 23:2881–2887. [PubMed: 17881408]

Shin J, Bossenz M, Chung Y, Ma H, Byron M, Taniguchi-Ishigaki N, Zhu X, Jiao B, Hall LL, Green MR, et al. Maternal Rnf12/RLIM is required for imprinted X-chromosome inactivation in mice. Nature. 2010; 467:977–981. [PubMed: 20962847]

Shin J, Wallingford MC, Gallant J, Marcho C, Jiao B, Byron M, Bossenz M, Lawrence JB, Jones SN, Mager J, et al. RLIM is dispensable for X-chromosome inactivation in the mouse embryonic epiblast. Nature. 2014; 511:86–89. [PubMed: 24870238]

Trapnell C, Pachter L, Salzberg SL. TopHat: discovering splice junctions with RNA-Seq. Bioinformatics. 2009; 25:1105–1111. [PubMed: 19289445]

Vallaster MP, Kukreja S, Bing XY, Ngolab J, Zhao-Shea R, Gardner PD, Tapper AR, Rando OJ. Paternal nicotine exposure alters hepatic xenobiotic metabolism in offspring. Elife. 2017; 6

Wang F, Shin J, Shea JM, Yu J, Boskovic A, Byron M, Zhu X, Shalek AK, Regev A, Lawrence JB, et al. Regulation of X-linked gene expression during early mouse development by Rlim. Elife. 2016; 5

Zhu LJ. Integrative analysis of ChIP-chip and ChIP-seq dataset. Methods in molecular biology. 2013; 1067:105–124. [PubMed: 23975789]

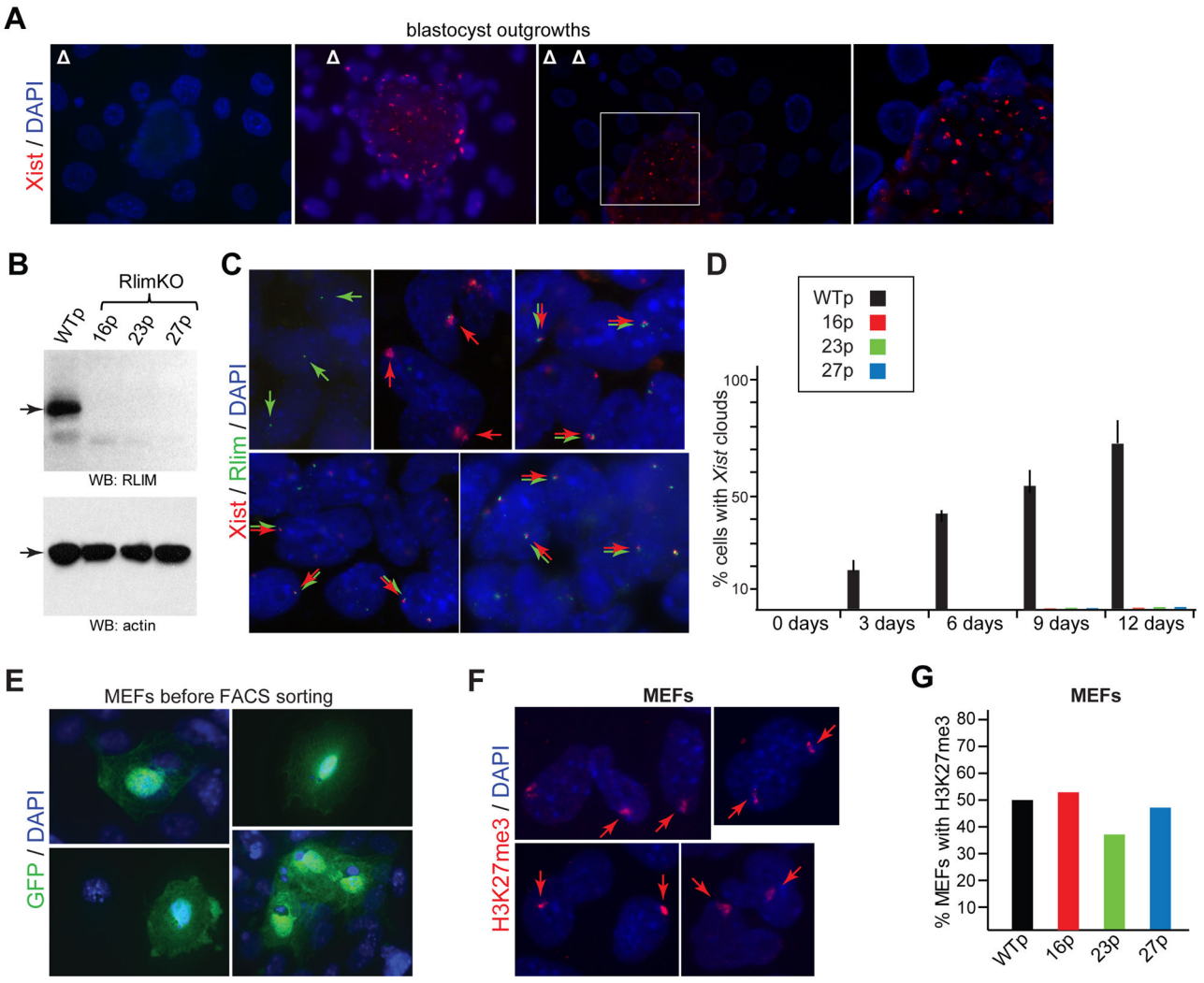

Figure 1. *Rlim*-independent XCI in female ESCs *in vivo*

A) Development of *Xist* clouds in ICM of female blastocyst outgrowths lacking maternal and embryonic RLIM. RNA FISH on E4 blastocyst outgrowths cultured for 72h using *Xist* as probe. Embryos were generated by crossing Δ/Y males with either SC-cKO$_m$/Δ$_p$ or fl/fl females. Boxed area (Δ$_m$/Δ$_p$ embryo) is shown in higher magnification in the right panel. Focus in images is on cells in the ICM. Embryos were genotyped after image recording. **B)** Generation of female *Rlim*KO ESC lines via CRISPR/Cas9. Western blot of undifferentiated WTp and *Rlim*KOp lines using antibodies against RLIM (top) or β-actin (bottom). **C)** XCI upon RA-differentiation of ESCs is *Rlim*-dependent. RNA-FISH on 6d RA-differentiated ESCs using *Xist* (red) and *Rlim* (green) as probes. Note side-by-side *Xist* and *Rlim* transcription foci but no *Xist* clouds in *Rlim*KO ESCs. **D)** XCI profile in ESCs RA-differentiated up to 12 days. Data reflect two independent experiments with >500 cells counted for each ESC line and time point. Error bars indicate standard error of the mean (SEM). **E)** Approx. 12–15 undifferentiated GFP-tagged ESCs were microinjected into E3.5 blastocysts, which were surgically placed into the uteri of pseudo pregnant females. MEFs were prepared from E12.5 embryos and stained with GFP antibodies. **F)** FACS-sorted WT

and KO MEFs were stained with antibodies against H3K27me3. Arrows: H3K27me3 foci marking the Xi. **G)** Summary of H3K27me3 foci in F); n>150 cells each. See also Figure S1.

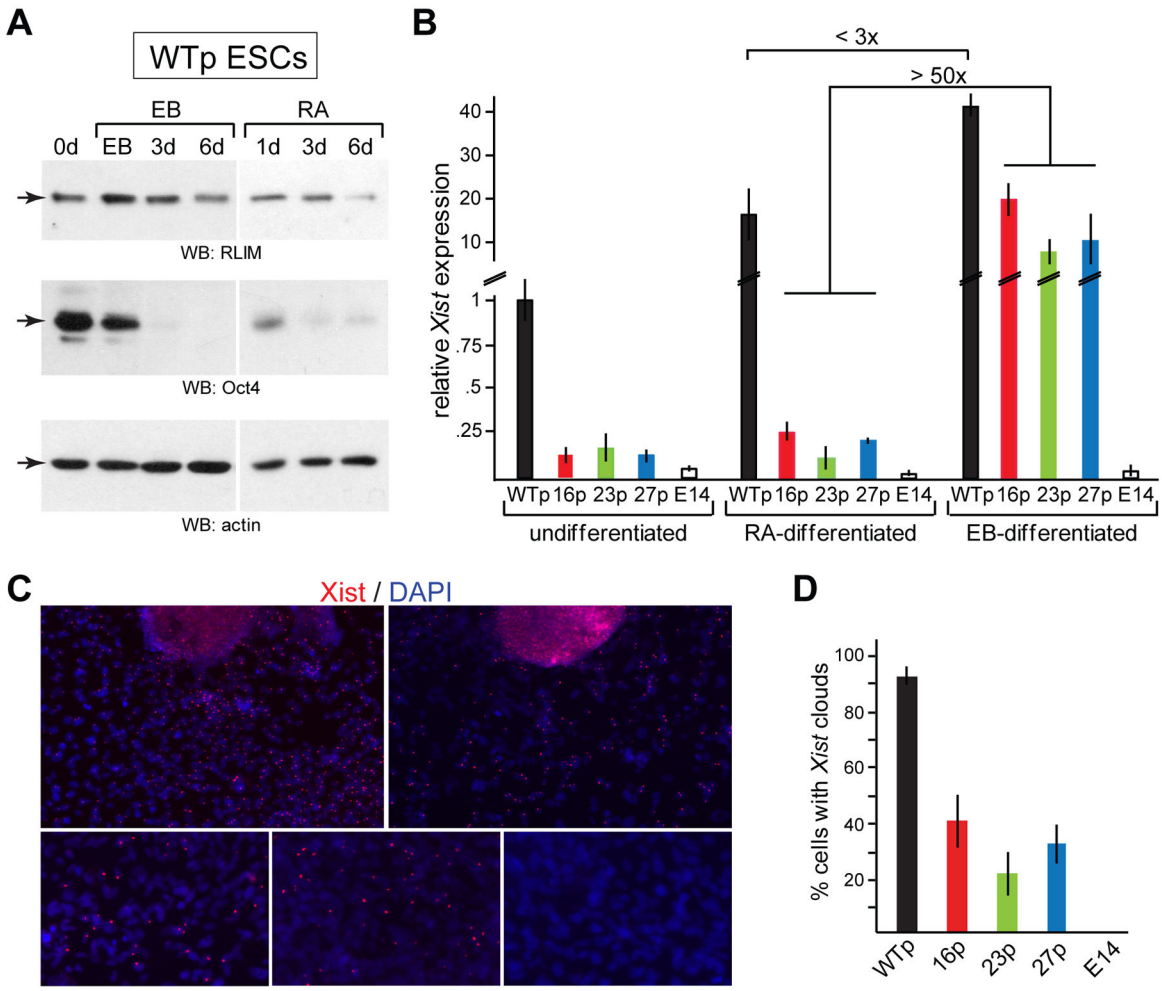

Figure 2. *Rlim*-dependent and –independent XCI pathways exist in ESCs

A) WT ESCs were split and *in vitro* differentiated in parallel either by EB or RA. Protein extracts were prepared at various time points during differentiation. The same Western blot was hybridized with antibodies against RLIM, OCT4 and β-actin. Note that Oct4 levels drop dramatically by 3d, while RLIM levels are not significantly downregulated by 6d. **B)** Comparison of *Xist* RNA levels in undifferentiated ESCs and after 6d RA-or EB-differentiation via ssRT-qPCR (control: E14 male ESCs; *Xist* levels of undifferentiated WTp cells are set to 1). Data represent three independent experiments. Note that *Xis*t levels are < 3× higher in EB-differentiated WTp ESCs when compared to RA-differentiation, but > 50× for all *Rlim*KOp ESCs. **C)** Formation of *Xist* clouds in (6d) EB-differentiated *Rlim*KOp ESCs in RNA FISH using *Xist* as probe. Representative images are shown. **D)** Summary of three independent experiments as shown in (C). *Xist* clouds in ESCs of 10 EBs were evaluated with >100 cells counted per EB. Error bars indicate standard error of the mean (SEM).

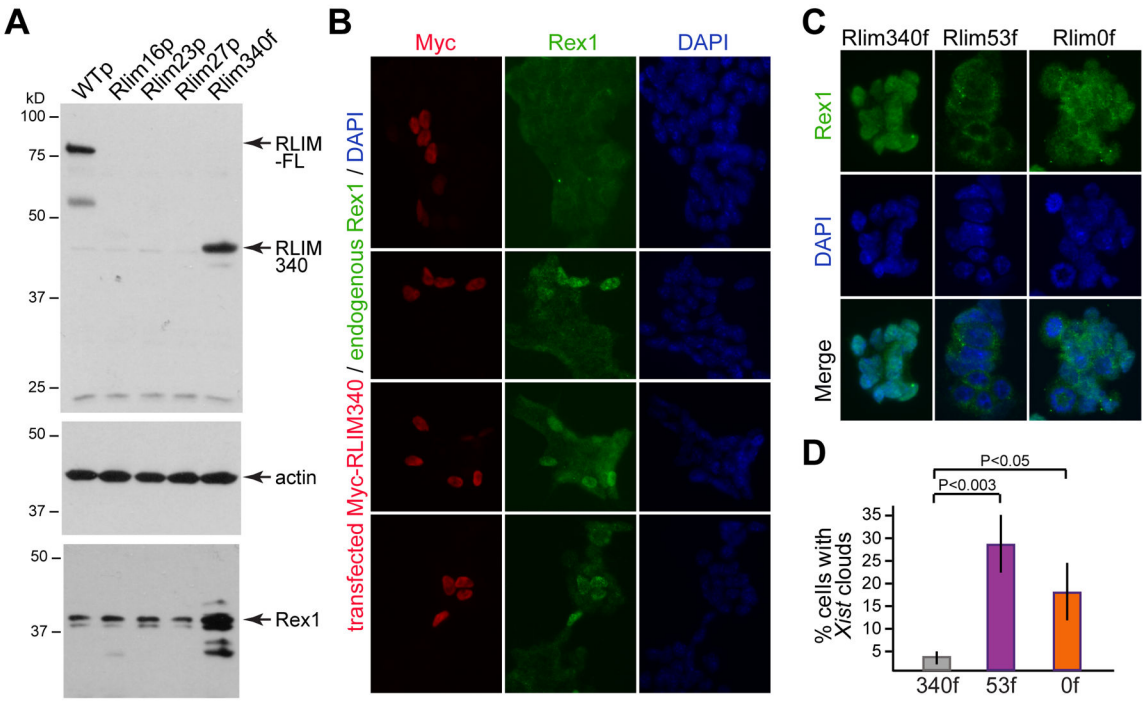

Figure 3. A truncated RLIM340 protein is expressed in *Rlim*340f ESCs

A) Western blot on undifferentiated ESCs was consecutively hybridized with RLIM-M, β-actin and REX1 antibodies. Note the presence of RLIM340 in *Rnf12*KO (*Rlim*340f) ESCs. Moreover, REX1 levels are elevated in *Rlim*340f ESCs but not in *Rlim*KOp ESCs. **B)** Forced expression of Myc-tagged RLIM340 in *Rlim*KOp ESCs leads to nuclear accumulation of endogenous REX1. **C)** RLIM340 traps REX1 in the nucleus. ICC on undifferentiated ESCs using REX1 antibodies. Note mostly nuclear localization of REX1 in *Rlim*340f but not in *Rlim*53f and *Rlim*0f ESCs. **D)** Presence of RLIM340 inhibits XCI efficiency. Summary of *Xist* clouds from three independent experiments in *Rlim*340f, *Rlim*53f and *Rlim*0f ESCs EB-differentiated for 6d. From each experiment *Xist* clouds in ESCs of 10 EBs were evaluated with >100 cells counted per EB. Error bars indicate SEM. See also Figure S2.

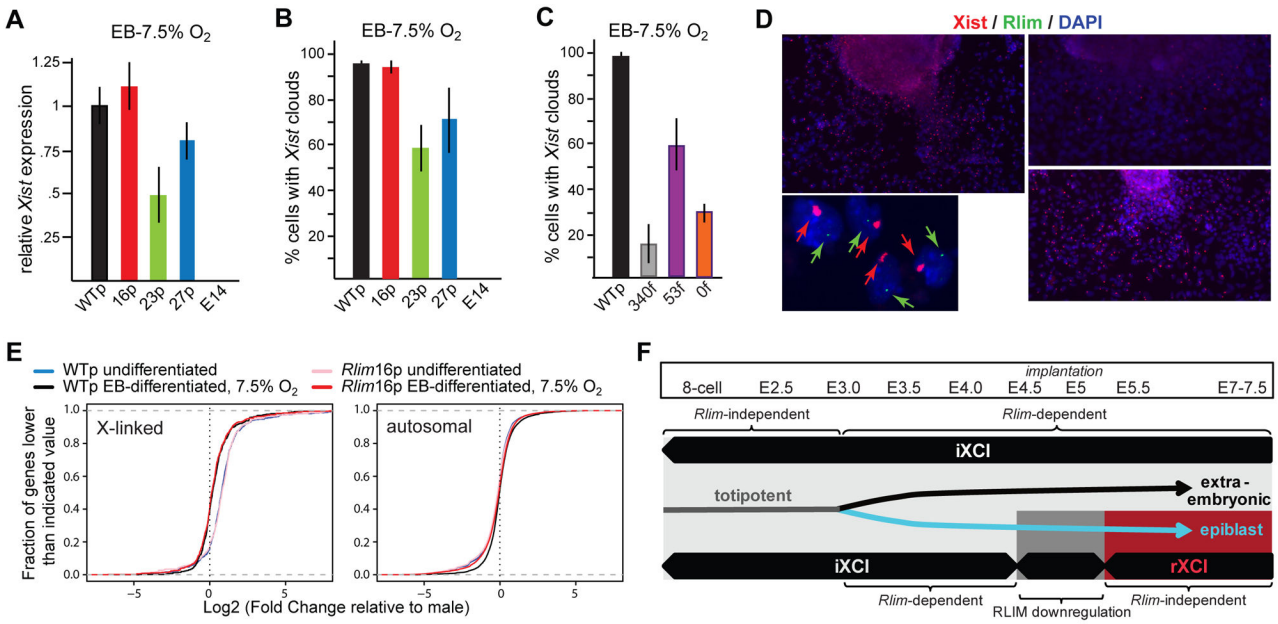

Figure 4. RLIM-independent XCI in ESCs *in vitro*

A) *Xist* levels (ssRT-qPCR) in ESCs, EB-differentiated and cultured for 6d in 7.5% O_2. Results represent three independent experiments. *Xist* levels of differentiated WTp cells are set to 1. **B, C)** Summary of comparison of *Xist* cloud formation in ESCs (EB-differentiated in 7.5% O_2) cultured for 6d as determined by RNA FISH using *Xist* as probe. Genotypes are indicated. *Xist* clouds were counted in two independent experiments (10 EBs with >100 cells counted per EB). **D)** Representative images of RNA FISH on 6d EB-differentiated ESCs (7.5% O_2). Lower left panel shows *Rlim*16p co-hybridized with *Xist* (red) and *Rlim* (green) probes in higher magnification. **E)** *Rlim*-independent chromosome wide X-silencing *in vitro*. Log2 transformed RNA-seq data obtained from two biological replicates of undifferentiated and differentiated (6d EB-differentiation; 7.5% O_2) each of WT, *Rlim*16p and E14 ESCs were compared for F/M expression level ratios from 550 X-linked genes (left panel) and 13526 autosomal genes (right panel). **F)** Summary of XCI during female mouse embryogenesis and the dependence on *Rlim*. Embryonic stages, iXCI (light grey) and rXCI (red) and XCR (dark grey) as well as embryonic cell lineages are indicated (grey, totipotent cell lineage; black, extraembryonic cell lineages; blue, epiblast cell lineage). Error bars in A–C indicate standard error of the mean (SEM). See also Figure S3.